SOLUTION MINING RESEARCH INSTITUTE

679 Plank Road
Clifton Park, NY 12065, USA

Telephone: +1 518-579-6587
www.solutionmining.org

Technical Conference Paper

1965 – 2025

Uncertainty Propagation Method Applied to Nitrogen-Brine Mechanical Integrity Test Analysis

Matteo Scapolan

RESPEC, Montreal, Canada

Sophie Minas

RESPEC Consultant to WSP USA, Montreal, Canada

SMRI Spring 2025 Technical Conference
27-29 April 2025
Wilhelmshaven, Germany

Solution Mining Research Institute Spring 2025 Technical Conference

Wilhelmshaven, Germany 27-30 April 2025

Uncertainty Propagation Method Applied to Nitrogen-Brine Mechanical Integrity Test Analysis

Matteo Scapolan, RESPEC, Montreal, Canada

Sophie Minas, RESPEC Consultant to WSP USA, Montreal, Canada

Abstract

Solution-mined salt caverns are commonly used to store liquid and gaseous products underground. Mechanical Integrity Tests (MITs) are conducted periodically to ensure that the cavern system is tight, secure, and capable of safely containing the stored product. Through this test, leakage is assessed to determine if the cavern is safe to operate, as a leaking cavern presents an unacceptable risk to the owner as well as the public.

In the US, the most commonly performed MIT is the Nitrogen-Brine Interface MIT. The Nitrogen-Brine Interface test is executed by injecting nitrogen into the annulus between the cemented production casing and the brine injection tubing and by running temperature and density logs on two occasions, separated by a specified time interval. The wellhead pressure is also measured continuously. At the conclusion of MIT logging, a calculated leak rate (CLR), comparing the total nitrogen gas volume at the test start and end is obtained along with an associated uncertainty known as the minimum detectable leak rate (MDLR).

In this paper a new approach to the Nitrogen-Brine Interface MIT analysis is developed in which a statistical tool called the "uncertainty propagation method" is implemented. The proposed approach consists of a standard CLR computation coupled with a revised procedure for the determination of the MDLR. Since the uncertainty of the CLR depends on the accuracy of the measured quantities (pressure, temperature, interface depth, test volume, etc.), it is possible to apply the uncertainty propagation method, which is widely used to compute uncertainties in quantities that are not measured directly, but rather calculated through a set of measurands.

While the traditional approach to the MDLR calculation relies only on the uncertainty in the interface detection, in this paper the uncertainty of all measured quantities is taken into account. This includes the measures used to determine the test volume (annulus area, nitrogen flow during borehole strapping procedure and interface depth) and the in-situ density (surface pressure and downhole temperature). This allows for an evaluation of all uncertainty contributions, not only determining an accurate value for the MDLR, but also quantifying the influence of each instrument uncertainty.

This paper provides an overview of the typical US Nitrogen-Brine Interface MIT, together with the new analysis method. Case study examples of storage cavern MITs are provided, comparing the traditional method to the novel approach.

Key words: MIT, Storage, Uncertainty Propagation, Error Propagation.

1 Introduction

In this paper the nitrogen-brine Mechanical Integrity Test (MIT) is analyzed, with the main goal of assessing the uncertainty in the determination of the leak rate. A secondary objective is to pair this assessment with a suitable pass/fail criteria. Even though several variations of the test are implemented around the world, this paper addresses the approach most commonly used in North America. Since the main principles, and to some extent even the test procedure are the same, most of the work done in this paper can be easily translated to other MIT variations.

The traditional MIT procedure described in Section 2 is analyzed to identify all sources of uncertainty. In Section 3 the uncertainty propagation method, used in this paper to calculate the leak rate uncertainty, is described from a conceptual standpoint. In Section 4 this approach is applied to the nitrogen-brine MIT, providing the theoretical formulation and all the equations needed for its implementation. All sources of uncertainty identified are tackled in this section while maintaining the two key concepts of (1) limiting the simplifying assumptions as much as possible and (2) using measured quantities as the ultimate source of uncertainty.

Section 5 reports the results of the application of the uncertainty propagation method to real-world examples. Additionally, in this section an approximated approach is proposed, which greatly simplifies the formulation while not significantly compromising the accuracy in the calculation of the leak uncertainty. Finally, in Section 6 comparisons between the traditional approach and the proposed one are made, before the conclusions in Section 7.

2 Traditional Nitrogen-Brine MIT

As described in [1] and [2], the most commonly performed MIT in North America is the nitrogen-brine interface test. The purpose of the MIT is to assess if the storage system demonstrates the mechanical integrity required for hydrocarbon storage. A nitrogen-brine interface test consists of the following steps in summary: (1) pressurizing the cavern with brine to a given test pressure, (2) injecting nitrogen into the well to set the nitrogen-brine interface below the production casing shoe, (3) recording nitrogen and brine wellhead pressures and the nitrogen-brine interface depth over the test period.

To prepare for the start of an MIT, the cavern is pressurized by injecting saturated brine into the hanging string of the well. Brine pressures are monitored at the wellhead until the pressure is stabilized at the targeted test pressure and pressure decline rates are less than 10 psi/day. Once these conditions are met, base density (gamma-gamma) and temperature logs are run in the well. Nitrogen is then injected into the well at a temperature close to the average wellbore temperature measured by base temperature log. At first, nitrogen is injected to a depth above the production casing shoe where a cemented casing test is performed (as illustrated in [1]). Following the casing test, nitrogen is injected below the production casing shoe depth and to the planned interface depth for the casing shoe test. The uncertainty of the casing shoe test is the focus of this paper. During nitrogen injection, nitrogen and brine wellhead pressures are measured and the nitrogen flow is measured via a flow meter while the nitrogen-brine interface depth is tracked with the density tool. This allows for a calculation of the size of the borehole. After a stabilization period, the test is initialized with an initial temperature and density log. The test is finalized after the planned test duration with a set of final temperature and density logs. Nitrogen and brine wellhead pressures are continuously monitored during the entire test.

Based on the measured data, the mass of nitrogen contained in the well is calculated at the test start and test end. A calculated leak rate (CLR) of gas from the cavern is then calculated as the change in gas inventory over the test period. A CLR is expressed in units of flow, such as million standard cubic feet per day, where a standard cubic foot is the mass of gas that occupies a cubic foot of volume at standard temperature and pressure conditions. A Minimum Detectable Leak Rate (MDLR) is calculated using Equation 1.

$$MDLR = \frac{A_n \, \delta h_n}{\Delta t} \tag{1}$$

where A_n is the unit volume of the borehole, δh_n is resolution of the interface detection, and Δt is the test duration. The MDLR is usually computed in bbls/year, using average borehole conditions.

The test is considered as passed if (1) the CLR is lower than the MDLR and (2) the MDLR is lower than a Maximum Allowable Leak Rate (MALR), usually fixed at 1000 bbls/year (≈160 m^3/year) at average borehole conditions. Figure 1 illustrate some examples of possible MIT results.

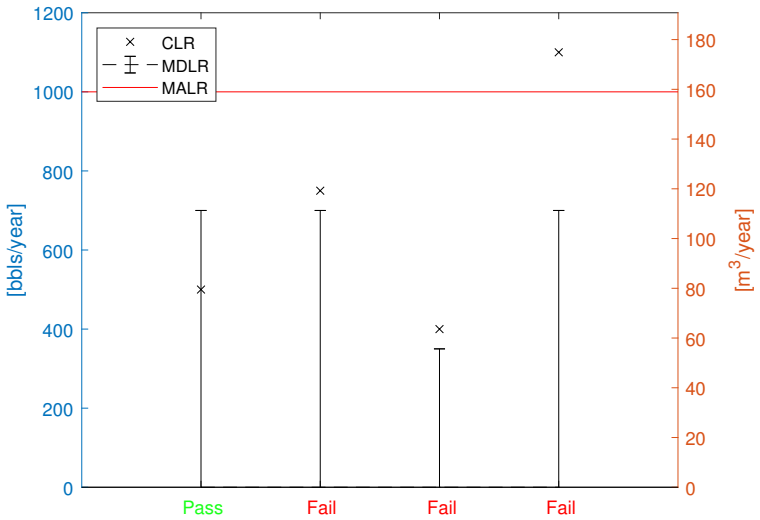

Figure 1: Traditional MDLR Example.

Analyzing Figure 1 it is clear how the MDLR is not used as CLR uncertainty (nor is it defined in that way). Moreover, while the two pass conditions in practice limit the amount of possible leak, there is one possible drawback: the third example represents a failed test, even though both CLR and MDLR are lower than the first example, in which the test passes. The current criteria in fact penalize more accurate tests (lower MDLR) and in general it is counterproductive to further reduce the MDLR once MDLR<MALR. This is likely due to the fact that the test is designed to pass only when no leaks are detected (CLR<MDLR), with an additional constraint (MDLR<MALR) limiting the maximum leak rate.

3 Uncertainty Propagation Method

Every measured value is associated with an uncertainty range or a range of probable error. A measured value can be considered to be a sample from an infinite set of possible measurements. The probability distribution curve shown in figure 2 illustrates the typical situation for experimental measurements. The probability distribution curve typically has a bell-shaped curve that follows a Gaussian or Normal distribution. The peak in the distribution curve indicates the most probable measured value, which is also the mean value of the distribution. Individual samples will tend to randomly scatter about the most probable value.

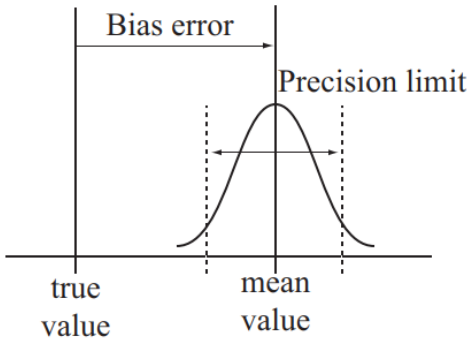

Figure 2: Probability distribution curve for a measurand.

Measurement devices have an associated error that includes components of (1) device bias error and (2) device random precision error. The offset between the true value and the mean of the probability distribution is called the bias error and can be reduced through instrument calibration. Often one does not know the actual bias error, but has an estimate of what range the bias error may be within. For example the bias error of a thermocouple is typically stated as $\pm 1^{\circ}$C. Precision error is the random error associated with the difference between a single sample and the mean of the probability distribution and may be caused by small fluctuations (e.g. temperature or electrical current) in the measurement region. The precision limit describes the expected upper limit for the precision error, and is stated to a certain confidence interval, usually 95$\%$ for a Normal distribution. When this is used to calculate the uncertainty of a dependent variable, the uncertainty of the dependent variable matches that of the tool confidence interval.

The overall uncertainty is the root-sum-square of the bias and precision errors,

$$\delta X = \sqrt{B^2 + P^2} \tag{2}$$

where δX is the uncertainty, B is the bias limit, and P is the precision limit.

Unfortunately, instrument manufacturers do not generally provide uncertainty measurements in terms of bias and precision limits, but are often given in terms of linearity, hysteresis, sensitivity, zero shift, and repeatability among other possible definitions. In general, when an instrument is specified to have a certain "accuracy", usually in terms of percent of the full scale value of the instrument, this is associated with the bias limit. Repeatability is associated with the precision limit. The standard method for estimating the precision error due to scale resolution is to assume the precision limit is 1/2 the smallest division (or 1/2 the smallest digit for digital readouts). Precision errors will occasionally be estimated directly from data samples, when a series of measurements are repeated.

Often, quantities of interest are not directly measured. It is common to measure a set of measurands that allows for the calculation of another variable using a known equation. The propagation of uncertainty (or propagation of error), expresses the idea that uncertainties in measured quantities beget uncertainties in quantities calculated from them. Consider a general example where variable R is dependent on a set of independent, measured, variables $(x_1, x_2, ...x_m)$, as per Equation 3.

$$R = R(x_1, x_2, ..., x_m) \tag{3}$$

Assuming the uncertainty has a normal probability distribution, the uncertainty in the dependent variable, R, may be determined from the known uncertainty of each independent variable. The uncertainty in R is calculated using the equation derived in [3]:

$$\delta R = \sqrt{\left(\frac{\partial R}{\partial x_1}\right)^2 \delta x_1^2 + \left(\frac{\partial R}{\partial x_2}\right)^2 \delta x_2^2 + ... + \left(\frac{\partial R}{\partial x_m}\right)^2 \delta x_m^2}$$

where δR represents the uncertainty in R and the uncertainties in the measured quantities are $\delta x_1, ..., \delta x_m$. An example of the uncertainty propagation approach applied to calculating the volume a cube containing a cylindrical hole can be found in [4].

4 Uncertainty Propagation Method Applied to Nitrogen MITs

In this section, the uncertainty propagation method is applied to the leak rate calculation in nitrogen-brine MITs. Firstly, the equations used to compute the Calculated Leak Rate (CLR) are given in section 4.1 as per current MIT standard and the borehole strapping procedure is described in section 4.2.

In section 4.3 the derivation of the CLR uncertainty, represented as δCLR is described in detail. The quantity called MDLR (Minimum Detectable Leak Rate) is sometimes considered as the uncertainty of the CLR, but in this paper it is kept separate from δCLR. A comparison between MDLR and δCLR is provided in section 6.

4.1 Calculated Leak Rate

The Calculated Leak Rate (CLR) is computed as the difference in the mass of gas or gas inventory between an initial and a final log as shown in Equation 4. Quantities m_I and m_F are the inventories computed using the initial and final logs respectively and Δt is the time interval between them.

$$\mathrm{CLR} = \frac{m_F - m_I}{\Delta t} \tag{4}$$

Equation 5 is used to compute both m_F and m_I. An important concept highlighted in Equation 5 is that the tested volume is discretized into a set of n vertical depth intervals, from surface ($i = 0$) to the nitrogen-brine interface ($i = n$). This is necessary because the density of nitrogen changes significantly with depth. Temperature logs are performed both at the beginning and at the end of the test, allowing for an accurate computation of the conditions at each vertical interval i.

$$m = \sum_{i=0}^{n} \rho_i \, V_i \tag{5}$$

4.2 Borehole Strapping

During a nitrogen-brine MIT only the upper portion of the cavern including the borehole and the upper portion of the cavern neck is tested, starting from the wellhead up to just below the casing shoe (CS). Contrary to a gas-filled MIT, where the tested volume is determined via sonars, in a nitrogen-brine MIT a procedure commonly referred to as *borehole strapping* is performed; this operation includes simultaneous recording of the volume of injected nitrogen and interface position. This, together with the knowledge of the well completion and piping diameters, allows for the computation of the tested volume.

The volume of a vertical increment V_i can still be expressed as the multiplication between its height h_i and its corresponding cross-sectional area A_i, where:

- The height is arbitrarily defined and contains no uncertainty, except for the vertical increment immediately above the interface.
- The cross-sectional area can be computed based on:
  - The pipe diameters above the casing shoe.
  - The nitrogen flow below the casing shoe.

Equation 6 defines the volume of each vertical depth increment i, using either the volume of the annular space (above CS) or the measured injected nitrogen volume (below CS).

$$V_i = h_i \, A_i \quad \text{where} \begin{cases} A_i &= \frac{\pi}{4}\left(d_{O,i}^2 - d_{I,i}^2\right) \quad \text{above CS } (i < n_{CS}) \\ A_i &= \frac{\rho_{WH,i} \; V_{WH,i} \; dt_i}{\rho_i \; h_i} \qquad \text{below CS } (n_{CS} < i \leq n) \end{cases} \tag{6}$$

The differentiation between the nitrogen density at the wellhead $\rho_{WH,i}$ and the nitrogen density at the interface ρ_i is necessary to properly calculate the volume effectively occupied by the injected nitrogen.

4.3 Leak Rate Uncertainty

The uncertainty in the CLR, here named $\delta\mathrm{CLR}$, is computed by propagating the uncertainty of measured quantities. Firstly, the CLR is defined and expressed as a function of different independent variables.

While it is always possible to obtain an equation for the CLR using as independent variables the measured quantities directly (e.g. pressure, temperature, interface depth), it is often more convenient to use a different set of independent variables with a more direct physical meaning. This results in a two-step process for the computation of the CLR uncertainty, where:

1. Step 1: compute uncertainty of CLR with respect to the selected independent variables.

2. Step 2: compute uncertainty of the selected independent variables with respect to the measured quantities.

The proposed approach allows for a simpler formulation and highlights the influence of variables of interest. Step 2 may be repeated several times to obtain the uncertainty with respect to measured variables.

Starting from Equation 4, it is possible to fulfill step 1 by writing the CLR as per Equation 7, where the independent variables are selected as density and volume of each interval, for both initial and final logs.

$$CLR = \frac{\sum_{i=0}^{n_I} \rho_{I,i}\ V_{I,i} - \sum_{j=0}^{n_F} \rho_{F,j}\ V_{F,j}}{\Delta t} \tag{7}$$

Two main assumptions can be made to simplify the formulation:

1. The position of the interface does not vary significantly between initial and final logs. While the interface is not to be considered fixed, it can be assumed that the discretization of the depth can be performed using the same number of intervals, leading to $n_I = n_F$.

2. Since a single borehole strapping is used for both logs, the interval volume is identical for all depth intervals for both initial and final logs, except for the last interval volume, which depends on the interface depth. This can be formulated as $V_{I,i} = V_{F,i} = V_i \quad \forall\ i < n$. Additionally $V_{I,n} = A_n\ h_{I,n}$ and $V_{F,n} = A_n\ h_{F,n}$, where A_n is the unitary volume of the cavern at the interface, usually reported in $\mathrm{ft}^3/\mathrm{ft}$, can be computed as per Equation 6.

This leads to a reformulation of Equation 7 as Equation 8 hereafter.

$$CLR = \frac{\sum_{i=0}^{n-1} (\rho_{I,i} - \rho_{F,i})\ V_i + (\rho_{I,n}\ h_{I,n} - \rho_{F,n}\ h_{F,n})\ A_n}{\Delta t} \tag{8}$$

The number of independent variables is therefore $3 \times n + 5$, where n is the number of depth intervals used. Each independent variable has its own uncertainty, whether it is a directly measured quantity or a calculated one. The overall CLR uncertainty ($\delta\mathrm{CLR}$) is defined in Equation 9 as the sum of all the independent variable uncertainties, each one multiplied by the partial derivative of the CLR with respect to the corresponding variable.

$$\delta\mathrm{CLR} = \sqrt{\begin{aligned}&\sum_{i=0}^{n-1} \left(\frac{\partial \mathrm{CLR}}{\partial \rho_{I,i}}\right)^2 \delta\rho_{I,i}^2 + \left(\frac{\partial \mathrm{CLR}}{\partial \rho_{I,n}}\right)^2 \delta\rho_{I,n}^2 + \left(\frac{\partial \mathrm{CLR}}{\partial h_{I,n}}\right)^2 \delta h_{I,n}^2 + \\ &+ \sum_{i=0}^{n-1} \left(\frac{\partial \mathrm{CLR}}{\partial \rho_{F,i}}\right)^2 \delta\rho_{F,i}^2 + \left(\frac{\partial \mathrm{CLR}}{\partial \rho_{F,n}}\right)^2 \delta\rho_{F,n}^2 + \left(\frac{\partial \mathrm{CLR}}{\partial h_{F,n}}\right)^2 \delta h_{F,n}^2 + \\ &+ \sum_{i=0}^{n-1} \left(\frac{\partial \mathrm{CLR}}{\partial V_i}\right)^2 \delta V_i^2 + \left(\frac{\partial \mathrm{CLR}}{\partial A_n}\right)^2 \delta A_n^2\end{aligned}} \tag{9}$$

The partial derivatives are easily obtained analytically and listed in Equation 10.

$$\frac{\partial \mathrm{CLR}}{\partial \rho_{I,i}} = \frac{V_i}{\Delta t} \tag{10a}$$

$$\frac{\partial \mathrm{CLR}}{\partial \rho_{F,i}} = -\frac{V_i}{\Delta t} \tag{10b}$$

$$\frac{\partial \mathrm{CLR}}{\partial \rho_{I,n}} = \frac{h_n\ A_n}{\Delta t} \tag{10c}$$

$$\frac{\partial \mathrm{CLR}}{\partial \rho_{F,n}} = -\frac{h_n\ A_n}{\Delta t} \tag{10d}$$

$$\frac{\partial \mathrm{CLR}}{\partial h_{I,n}} = \frac{\rho_{I,n}\ A_n}{\Delta t} \tag{10e}$$

$$\frac{\partial \mathrm{CLR}}{\partial h_{F,n}} = -\frac{\rho_{F,n}\ A_n}{\Delta t} \tag{10f}$$

$$\frac{\partial \mathrm{CLR}}{\partial V_i} = \frac{\rho_{I,i} - \rho_{F,i}}{\Delta t} \tag{10g}$$

$$\frac{\partial \mathrm{CLR}}{\partial A_n} = \frac{\rho_{I,n}\ h_{I,n} - \rho_{F,n}\ h_{F,n}}{\Delta t} \tag{10h}$$

Only $\delta h_{I,n}$ and $\delta h_{F,n}$, which are uncertainties of measured quantities, are directly available, while other uncertainties have to be calculated in an additional step. Details of these calculations are provided in sections 4.3.1 through 4.3.4.

4.3.1 Density Uncertainty

The uncertainty in density can be evaluated after expressing density in terms of independent variables. In Equation 11, pressures ($p_{I,i}$ and $p_{F,i}$), temperatures ($T_{I,i}$ and $T_{F,i}$) and compressibilities ($Z_{I,i}$ and $Z_{F,i}$) are used as independent variables.

$$\begin{aligned} \rho_{I,i} &= \frac{p_{I,i}}{R_S\, T_{I,i}\, Z_{I,i}} \qquad \forall\, i = 0, \ldots, n \\ \rho_{F,i} &= \frac{p_{F,i}}{R_S\, T_{F,i}\, Z_{F,i}} \qquad \forall\, i = 0, \ldots, n \end{aligned} \tag{11}$$

Uncertainties $\delta\rho_{I,i}$ and $\delta\rho_{F,i}$ are defined as per Equation 12.

$$\delta\rho_{I,i} = \sqrt{\left(\frac{\partial\rho_{I,i}}{\partial p_{I,i}}\right)^2 \delta p_{I,i}^2 + \left(\frac{\partial\rho_{I,i}}{\partial T_{I,i}}\right)^2 \delta T_{I,i}^2 + \left(\frac{\partial\rho_{I,i}}{\partial Z_{I,i}}\right)^2 \delta Z_{I,i}^2} \tag{12a}$$

$$\delta\rho_{F,i} = \sqrt{\left(\frac{\partial\rho_{F,i}}{\partial p_{F,i}}\right)^2 \delta p_{F,i}^2 + \left(\frac{\partial\rho_{F,i}}{\partial T_{F,i}}\right)^2 \delta T_{F,i}^2 + \left(\frac{\partial\rho_{F,i}}{\partial Z_{F,i}}\right)^2 \delta Z_{F,i}^2} \tag{12b}$$

Temperatures $T_{I,i}$ and $T_{F,i}$ are measured directly at all depth intervals and the uncertainty of temperature measurements is that of the tool used. The partial derivatives appearing in Equation 12 are expressed in Equation 13 and are valid for both initial and final logs.

$$\frac{\partial\rho_i}{\partial p_i} = \frac{1}{R_S\, T_i\, Z_i} \tag{13a}$$

$$\frac{\partial\rho_i}{\partial T_i} = -\frac{p_i}{R_S\, T_i^2\, Z_i} \tag{13b}$$

$$\frac{\partial\rho_i}{\partial Z_i} = -\frac{p_i}{R_S\, T_i\, Z_i^2} \tag{13c}$$

4.3.2 Pressure Uncertainty

The pressure is typically measured only at the surface and calculated at all other depths based on temperature measurements.Two approaches can be used to evaluate the uncertainty in pressure:

1. Consider the average pressure of a depth interval as equal to the latest known value (top of the depth interval).
2. Consider the average pressure of a depth interval as an unknown value.

Using the first approach, the average pressure of depth interval i is defined as per Equation 14. This approach is simpler and is most commonly used.

$$p_i = p_{i-1} \frac{R_S\, T_i\, Z_i + g\, \Delta h_i}{R_S\, T_i\, Z_i} \tag{14}$$

The second approach, which is mathematically more accurate, uses Equation 15 to define p_i.

$$p_i = p_{i-1} \frac{R_S\, T_i\, Z_i + \frac{g\, \Delta h_i}{2}}{R_S\, T_i\, Z_i - \frac{g\, \Delta h_i}{2}} \tag{15}$$

Comparing Equation 14 and 15, it is clear that the smaller the depth interval, the closer the two definitions. From a practical point of view, the difference in the computed pressure is negligible.

Another consideration can be made regarding the compressibility Z_i. Because the compressibility is a function of the average pressure and temperature, its value is not known until p_i is computed. In practice,

the value of compressibility of the depth interval immediately above can be used with a very small error, since the compressibility of nitrogen does not vary significantly. This results in $Z_i \approx Z_{i-1}$ for the pressure computation. Equation 16 can then be used to define the pressure at depth interval i.

$$p_i = p_{i-1} \frac{R_S\, T_i\, Z_{i-1} + g\, \Delta h_i}{R_S\, T_i\, Z_{i-1}} \tag{16}$$

The uncertainty in the pressure can then by defined as per Equation 17, where the partial derivatives are expressed in Equation 18.

$$\delta p_i = \sqrt{\left(\frac{\partial p_i}{\partial p_{i-1}}\right)^2 \delta p_{i-1}^2 + \left(\frac{\partial p_i}{\partial T_i}\right)^2 \delta T_i^2} \tag{17}$$

$$\frac{\partial p_i}{\partial p_{i-1}} = 1 + \frac{g\, \Delta h_i}{R_S\, T_i\, Z_{i-1}} \tag{18a}$$

$$\frac{\partial p_i}{\partial T_i} = -\frac{p_{i-1}\, g\, \Delta h_i}{R_S\, T_i^2\, Z_{i-1}} \tag{18b}$$

In Equation 18 the compressibility is considered constant with respect to pressure and temperature. All simplifications introduced in this section amount to a very small, negligible error, which can be further reduced by discretizing the tested volume into a greater number of depth intervals.

4.3.3 Compressibility Uncertainty

The uncertainty in compressibility of a generic gas can be evaluated as proposed by [4], via a numerical perturbation method, whenever a closed-form solution does not exist. In the case of nitrogen gas, however, an approximation for the compressibility is given by [5] in a closed-form solution, as per Equation 19.

$$Z(p_i, T_i) = A(p_i, T_i)\, p_i^2 + B(p_i, T_i)\, p_i + C(p_i, T_i) \tag{19}$$

Considering pressure and temperature as measured variables, the uncertainty in the compressibility can be written as Equation 20, where the partial derivatives with respect to pressure and temperature are reported in Equation 21.

$$\delta Z_i = \sqrt{\left(\frac{\partial Z_i}{\partial p_i}\right)^2 \delta p_i^2 + \left(\frac{\partial Z_i}{\partial T_i}\right)^2 \delta T_i^2} \tag{20}$$

$$\frac{\partial Z_i}{\partial p_i} = 2\, A\, p_i + B \tag{21a}$$

$$\frac{\partial Z_i}{\partial T_i} = \frac{\partial A}{\partial T_i}\, p_i^2 + \frac{\partial B}{\partial T_i}\, p_i + \frac{\partial C}{\partial T_i} \tag{21b}$$

A, B and C are polynomials of T_i and are piece-wise constant with respect to p_i. For a specific value of pressure p_i these polynomials (reported in Equation 22) are a function of temperature only, which is why their partial derivatives with respect to the pressure do not appear in Equation 21a. Finally, the partial derivatives in Equation 21b can be easily obtained as per Equation 23.

$$\begin{cases} A &= A_0 + A_1\, T_i + A_2\, T_i^2 + A_3\, T_i^3 \\ B &= B_0 + B_1\, T_i + B_2\, T_i^2 \\ C &= C_0 + C_1\, T_i + C_2\, T_i^2 \end{cases} \tag{22}$$

$$\begin{cases} \frac{\partial A}{\partial T_i} = & A_1 + 2\, A_2\, T_i + 3\, A_3\, T_i^2 \\ \frac{\partial B}{\partial T_i} = & B_1 + 2\, B_2\, T_i \\ \frac{\partial C}{\partial T_i} = & C_1 + 2\, C_2\, T_i \end{cases} \tag{23}$$

4.3.4 Area Uncertainty

In section 4.3 the evaluation of the uncertainty in the tested volume was split into the uncertainty in height and the uncertainty in cross-sectional area. While the height uncertainty is addressed above, the area uncertainty is evaluated in this section. It is necessary to divide the cavern interval into two portions, one above the casing shoe ($i < n_{CS}$) and one between the casing shoe and the interface ($n_{CS} < i \leq n$). Equation 24 expresses the area in both portions, with Equation 24a pertinent at depths above the casing shoe and Equation 24b pertinent at depths below the casing shoe.

$$A_i = \frac{\pi}{4}\left(d_{O,i}^2 - d_{I,i}^2\right) \tag{24a}$$

$$A_i = \frac{\rho_{WH,i}\,\dot{V}_{WH,i}\,dt_i}{\rho_i\,h_i} \tag{24b}$$

The area uncertainty for the portion above the casing shoe is simple to compute, with the internal diameter of the outer pipe d_O and the external diameter of the inner pipe d_I as the only measured quantities. Equation 25 and Equation 26 report the main uncertainty equation and the partial derivatives respectively.

$$\delta A_i = \sqrt{\left(\frac{\partial A_i}{\partial d_{O,i}}\right)^2 (\delta d_{O,i})^2 + \left(\frac{\partial A_i}{\partial d_{I,i}}\right)^2 (\delta d_{I,i})^2} \tag{25}$$

$$\frac{\partial A_i}{\partial d_{I,i}} = \frac{\pi\,d_{O,i}}{2} \tag{26a}$$

$$\frac{\partial A_i}{\partial d_{O,i}} = -\frac{\pi\,d_{I,i}}{2} \tag{26b}$$

The computation of the area uncertainty for the portion of cavern below the casing shoe requires the evaluation of more mathematical terms. Aside from the measured flow of nitrogen $\dot{V}_{WH}$ at the wellhead and the interface depth h, the conditions at both the wellhead and interface need to be considered as measured quantities. Uncertainty is expressed as per Equation 27.

$$\delta A_i = \sqrt{\begin{array}{l}\left(\frac{\partial A_i}{\partial \rho_{WH,i}}\right)^2 \delta\rho_{WH,i}^2 + \left(\frac{\partial A_i}{\partial \rho_i}\right)^2 \delta\rho_i^2 + \left(\frac{\partial A_i}{\partial \dot{V}_{WH,i}}\right)^2 \delta\dot{V}_{WH,i}^2 + \\ + \left(\frac{\partial A_i}{\partial dt_i}\right)^2 \delta dt_i^2 + \left(\frac{\partial A_i}{\partial h_i}\right)^2 \delta h_i^2\end{array}} \tag{27}$$

The partial derivatives involved are reported in Equation 28, while the uncertainties of the measured variables can be obtained either directly from the tool or using procedures described in the other sections of this paper.

$$\frac{\partial A_i}{\partial \rho_{WH,i}} = \frac{\dot{V}_{WH,i}\,dt_i}{\rho_i\,h_i} \tag{28a}$$

$$\frac{\partial A_i}{\partial \rho_i} = -\frac{\rho_{WH,i}\dot{V}_{WH,i}\,dt_i}{\rho_i^2\,h_i} \tag{28b}$$

$$\frac{\partial A_i}{\partial \dot{V}_{WH,i}} = \frac{\rho_{WH,i}\,dt_i}{\rho_i\,h_i} \tag{28c}$$

$$\frac{\partial A_i}{\partial dt_i} = \frac{\rho_{WH,i}\dot{V}_{WH,i}}{\rho_i\,h_i} \tag{28d}$$

$$\frac{\partial A_i}{\partial h_i} = -\frac{\rho_{WH,i}\dot{V}_{WH,i}\,dt_i}{\rho_i\,h_i^2} \tag{28e}$$

5 Results

A total of 25 MITs were analyzed, representing a variety of conditions, as summarized hereafter. More details provided in Table A.1 and Table A.2 of Appendix A.

- Test duration between 24 hours and 387 hours
- CLR between $-560.42\frac{\text{scf}}{\text{day}}$ and $+425.72\frac{\text{scf}}{\text{day}}$ ($-18.81\frac{\text{kg}}{\text{day}}$ to $+14.29\frac{\text{kg}}{\text{day}}$)
- δCLR between $103.32\frac{\text{scf}}{\text{day}}$ and $1202.87\frac{\text{scf}}{\text{day}}$ ($3.47\frac{\text{kg}}{\text{day}}$ to $40.37\frac{\text{kg}}{\text{day}}$)

Commonly used values for the tool uncertainties are reported in Table 5.

Quantity	Uncertainty	Units	Uncertainty	Units
Pressure	1.25	psi	0.086	bar
Temperature	0.5	F	0.28	K
Interface	0.25-0.5	ft	0.076-0.152	m
Flow	2.0	%	-	-
Pipe diameter	0.25	in	0.0063	m

Table 5.1: Common uncertainties used.

The proposed pass/fail criterion respects the concept of uncertainty and can be expressed by Equation 29.

$$\text{CLR} + \delta\text{CLR} < \text{MALR} \tag{29}$$

This condition strongly enforces the Maximum Allowable Leak Rate (MALR), guaranteeing that the measured leak is below the accepted threshold. The confidence interval matches the one used for the measurement tools.

Figure 3 shows all the analyzed examples, with blue circles representing the CLR, blue bars representing the $\pm\delta$CLR and the red lines representing the MALR.

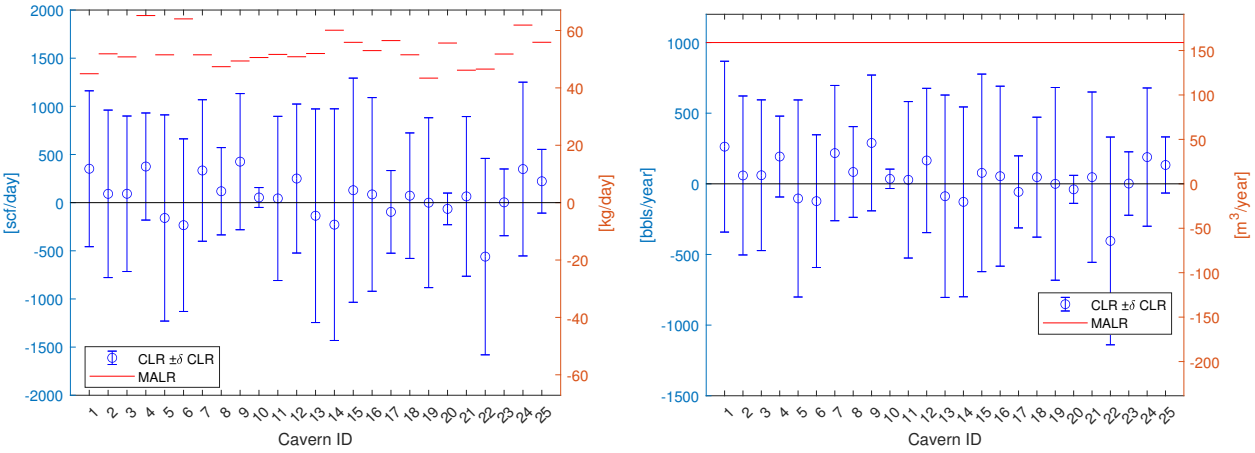

(a) Standard cubic feet per day.

(b) Barrels per year.

Figure 3: MIT Results, CLR and δCLR in blue, MALR in red.

Figure 3a is expressed in standard cubic feet per day, with the MALR that changes from cavern to cavern depending on the average borehole conditions. This is due to the fact that a fixed value of 1000 bbls in average borehole conditions results in a different amount of cubic feet in standard conditions. In Figure 3b

all results are expressed in bbls/year at average borehole conditions. This representation is useful because the MALR value is visually the same for all caverns.

All analyzed examples pass the test because $\mathrm{CLR} + \delta\mathrm{CLR} < \mathrm{MALR}$, and show no unacceptable leak. Moreover, $\mathrm{CLR} - \delta\mathrm{CLR} < 0$ for all cases, which signifies that no leak was detected. This last condition can be also written as $\mathrm{CLR} < \delta\mathrm{CLR}$, which is equivalent to the pass/fail criterion of the traditional approach $\mathrm{CLR} < \mathrm{MDLR}$.

5.1 Approximated Uncertainty

The uncertainty in the interface detection was by far the biggest contributor to the overall uncertainty. It is therefore possible to define an approximated value of δCLR from Equation 9 by (1) removing all terms not related to interface detection and (2) assuming a single, common value for nitrogen density at the interface between initial and final conditions, named $\overline{\rho}_n$. Equation 30 defines this quantity as $\delta\mathrm{CLR}^\star$, expressed in standard cubic feet (scf) by using the density in standard conditions ρ_{STD}.

$$\delta\mathrm{CLR} \approx \delta\mathrm{CLR}^\star = \sqrt{2}\frac{\overline{\rho}_n}{\rho_{STD}}\, A_n \frac{\delta h}{\Delta t} \tag{30}$$

Figure 4 shows a comparison between the proposed approximation ($\delta\mathrm{CLR}^\star$) and the full calculation that includes all terms (δCLR). The lines in Figure 4a are almost indistinguishable due to the small difference in values. This is further highlighted in Figure 4b in which the percentage error is illustrated.

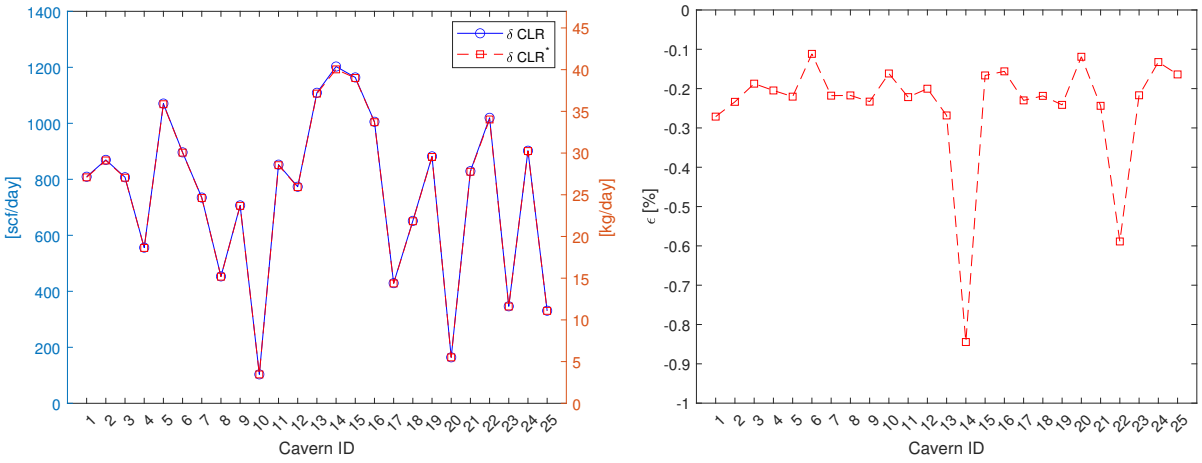

(a) Standard cubic feet per day.

(b) Percentage error with respect to $\delta\mathrm{CLR}$.

Figure 4: Comparison between $\delta\mathrm{CLR}$ and $\delta\mathrm{CLR}^\star$.

The average percentage error observed varied between 0.84% and 0.11%, with an average value of 0.24%. Based on these results and the simplicity of Equation 30, this approximated solution may be used. If desired, a 1% safety factor could be applied as a safety measure.

6 Comparison & Outlook

This section provides a comparison between the traditional approach to nitrogen MITs and the uncertainty propagation approach. Consistently with the rest of the paper, the term MDLR represents the concept of minimum detectable leak rate as defined by the traditional approach commonly practiced in North America. Conversely, the term δCLR represents the uncertainty in the computation of the calculated leak rate, as defined in this paper.

6.1 MDLR Comparison

The same set of 25 caverns was analyzed using the traditional approach. Test results are illustrated in Figure 5 and are analogous to the figures shown in Figure 3 for the Uncertainty Propagation Method.

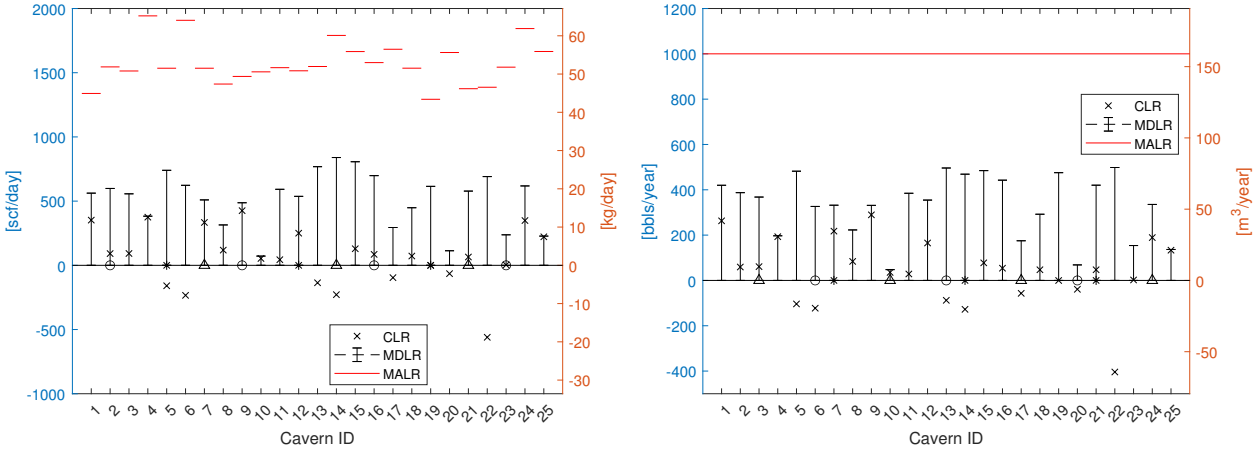

(a) Standard cubic feet per day.

(b) Barrels per year.

Figure 5: MIT Results, CLR and MDLR in black, MALR in red.

A direct comparison between MDLR and δCLR is complicated because of the different pass/fail criteria associated with the two quantities. Nevertheless, these two quantities are closely related, with the main differences identified as:

1. The MDLR uses the resolution of the interface detection only.
2. The MDLR is applied using average borehole conditions rather than interface conditions.
3. The MDLR equation implicitly assumes only a single measurement of the interface depth.

As explained in section 5.1, the first point does not cause any real discrepancy between MDLR and δCLR. Most of the observed difference between MDLR and δCLR relates to the second and third points. For this reason, it is possible to compare directly MDLR and δCLR*.

For the second point, in the MDLR calculation, a physical volume is defined by the incremental volume at the interface in which A_n is multiplied by the interface detection uncertainty δh_n. The gas contained in this volume is however assumed to be at average borehole conditions (with density ρ_{avg}), while it is in fact at interface conditions (with density $\overline{\rho}_n$).

For the third point, the MDLR calculation considers that the interface depth is measured only once, when in actuality the interface depth is measured twice (at test start and test end). The MDLR value should therefore be multiplied by $\sqrt{2}$ (see [4] for more details), assuming that similar conditions at the interface between initial and final logs allow for the use of a single, representative value for the interface density.

Taking into account all these factors, Equation 31 provides the expected relationship between MDLR and δCLR*.

$$\delta\mathrm{CLR}^\star \approx \sqrt{2}\frac{\overline{\rho}_n}{\rho_{avg}}\,\mathrm{MDLR} \tag{31}$$

Figure 6 provides a comparison between δCLR, its approximation δCLR* and the MDLR for all 25 examples considered. As demonstrated in Figure 6b, δCLR and MDLR differ by approximately 30%. This discrepancy is due to both $\sqrt{2}$ and the difference between interface conditions $\overline{\rho}_n$ and average borehole conditions ρ_{avg}.

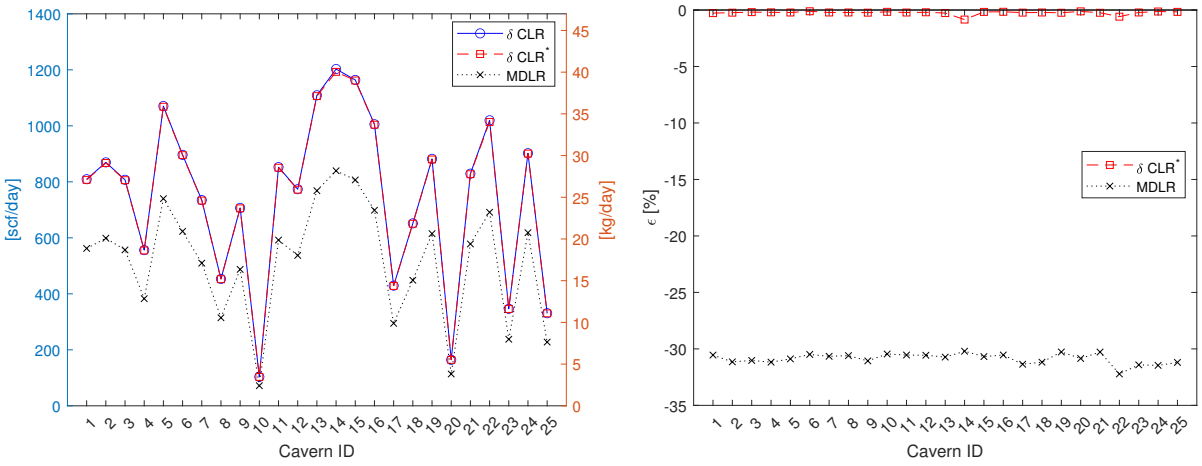

(a) Standard cubic feet per day.

(b) Percentage error with respect to $\delta\mathrm{CLR}$.

Figure 6: Comparison between $\delta\mathrm{CLR}$ (blue solid line, circle markers), $\delta\mathrm{CLR}^{\star}$ (red dashed line, square markers), and MDLR (black dotted line, cross markers).

6.2 Outlook

The proposed approach and pass/fail criterion have the benefit of rewarding more accurate tests. A lower value of $\delta\mathrm{CLR}^{\star}$ always makes it easier to pass the test, since the only condition is $CLR+\delta CLR^{\star} < MALR$.

Equation 30 gives an insight on how the test can be improved and how the $\delta\mathrm{CLR}^{\star}$ can be reduced. Figure 7 takes into consideration cavern 3 as an example and shows how the $\delta\mathrm{CLR}^{\star}$ varies when the two main factors in Equation 30 are considered.

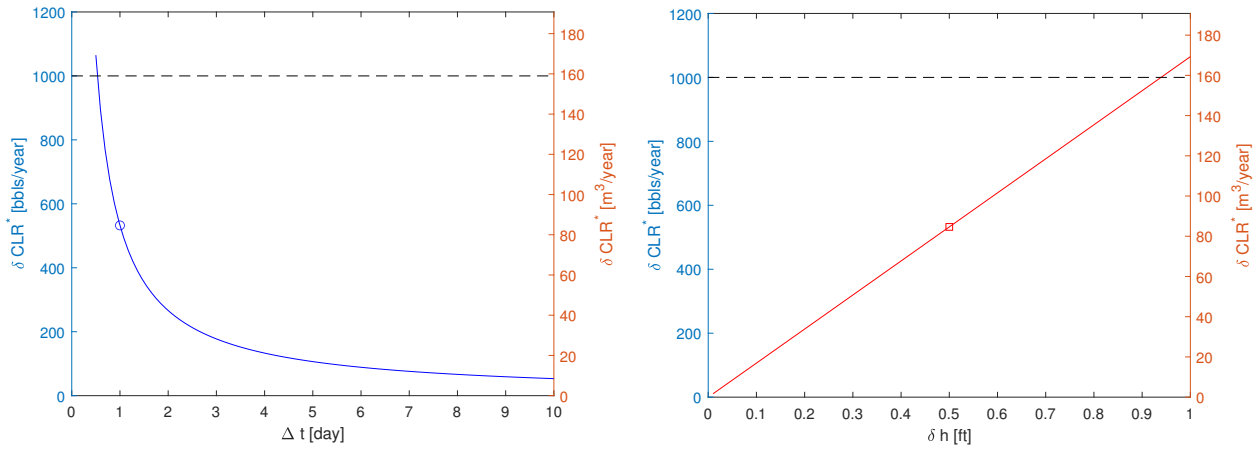

(a) $\delta\mathrm{CLR}^{\star}$ as a function of test duration.

(b) $\delta\mathrm{CLR}^{\star}$ as a function of interface detection uncertainty.

Figure 7: Cavern 3, $\delta\mathrm{CLR}^{\star}$ as a function of test duration (a) and interface detection uncertainty (b). Blue circle and red square represent nominal conditions, black dashed line represents MALR.

As illustrated in Figure 7a and as expected, longer tests result in higher accuracy. This is particularly relevant in countries that require an extended test duration.

As seen in Figure 7b, reducing the uncertainty in the interface detection δh results in a lower CLR uncertainty. Reducing δh can be done practically by (1) improving the tool accuracy and (2) repeating the interface measurement multiple times. Sonar-based tools (see [6]) are able to detect the interface with an accuracy of one order of magnitude superior to classic density-based tools (see [7]). They also allow for a continuous monitoring of the interface, further improving the CLR accuracy.

7 Conclusions

This paper analyzed the uncertainty in the CLR of nitrogen-brine Mechanical Integrity Test (MIT). This analysis was paired with the definition of a pass/fail criteria. The approach commonly used in North America was used a reference, but most of the conclusions of this paper are applicable to different variations as well.

The traditional MIT procedure was described in Section 2, where assumptions and uncertainty sources were identified. The uncertainty propagation method was conceptually introduced in Section 3 and applied to the nitrogen-brine MIT case in Section 4, where all the equations necessary for the implementation of this method were derived. In this phase the simplifying assumptions were limited as much as possible and the uncertainty sources were reduced to measured quantities.

The uncertainty propagation method was applied to 25 practical examples in Section 5. A simplified formulation was provided based on the observed results, which revealed that the interface detection uncertainty dominates the overall uncertainty. This approximation, proposed in Section 5.1, could be ultimately used in practice, showing a loss of accuracy of less than 1% in all tested examples.

Section 6 provided a comparison with the MDLR defined in the traditional approach and some general considerations regarding possible improvements to the test or its application to other variations of the nitrogen-brine MIT.

References

[1] T. Skaug Nils, L. Ratigan Joe, and C. Lampe Brandon. “A Critical Look at the Nitrogen/Brine Interface Mechanical Integrity Test”. In: *SMRI Technical Conference, York, UK* (2011).

[2] C. Lampe Brandon and L. Ratigan Joe. “Pitfalls of a Nitrogen-Brine Interface Mechanical Integrity Test”. In: *SMRI Technical Conference, San Antonio, TX, USA* (2014).

[3] Stephen J Kline. “Describing uncertainties in single-sample experiments”. In: *Mech. Eng.* 75 (1963), pp. 3–8.

[4] Sophie Minas. “A Novel Method for Gas Cavern Mechanical Integrity Test Analysis”. In: *SMRI Technical Conference, Detroit, MI, USA* (2023).

[5] *NOWSCO Technical Manual*. Nitrogen Oil Well Service Co. Box 3047, Houston, TX, USA, 1962.

[6] SOCON. *SoMIT® - TECHNOLOGY FOR PROCESSING GAS TIGHTNESS TESTS IN CAVITIES*. 2018. URL: https://socon.com/wp-content/uploads/2021/11/SOCON_SOMIT_Technology_EN.pdf (visited on 03/21/2025).

[7] SOCON. *Impulse-neutron-gamma tool*. 2018. URL: https://socon.com/wp-content/uploads/2021/11/SOCON_ING42SC_NG_Sonde_EN.pdf (visited on 03/21/2025).

A Appendix

Cavern ID	dh [ft]	dt [h]	CLR [scf/day]	δCLR [scf/day]	δCLR* [scf/day]	MDLR [scf/day]
1	0.50	24.00	352.04	809.28	807.09	562.08
2	0.25	48.03	91.51	869.46	867.42	598.62
3	0.50	24.00	92.21	807.32	805.81	556.85
4	0.50	24.12	375.10	556.04	554.90	382.69
5	0.50	27.60	-159.17	1070.57	1068.21	739.94
6	0.50	24.12	-233.82	896.29	895.29	623.01
7	0.50	48.48	333.92	734.81	733.21	509.54
8	0.50	24.05	118.46	453.24	452.26	314.57
9	0.50	72.07	425.72	706.87	705.23	487.30
10	0.50	24.08	53.36	103.32	103.15	71.86
11	0.50	72.10	43.80	852.38	850.49	592.04
12	0.50	24.07	250.35	773.59	772.04	537.15
13	0.50	24.00	-135.90	1109.07	1106.10	768.29
14	0.25	264.15	-228.47	1202.87	1192.71	839.51
15	0.50	72.07	129.16	1163.89	1161.95	806.77
16	0.50	24.03	85.27	1005.62	1004.05	698.50
17	0.50	24.07	-95.87	429.13	428.15	294.57
18	0.50	24.05	72.36	651.66	650.24	448.49
19	0.25	240.08	-0.33	881.95	879.83	614.95
20	0.50	24.12	-64.79	164.25	164.05	113.58
21	0.25	120.68	64.84	829.15	827.13	578.09
22	0.25	387.43	-560.42	1019.70	1013.70	691.17
23	0.50	24.08	3.15	346.48	345.73	237.64
24	0.50	24.03	348.80	902.13	900.93	618.31
25	0.50	24.00	222.15	330.78	330.24	227.58

Table A.1: Cavern Data of the 25 analyzed examples, US units.

Cavern ID	dh [m]	dt [h]	CLR [kg/day]	δCLR [kg/day]	δCLR* [kg/day]	MDLR [kg/day]
1	0.15	24.00	11.82	27.16	27.09	18.87
2	0.08	48.03	3.07	29.18	29.12	20.09
3	0.15	24.00	3.10	27.10	27.05	18.69
4	0.15	24.12	12.59	18.66	18.63	12.85
5	0.15	27.60	-5.34	35.93	35.86	24.84
6	0.15	24.12	-7.85	30.08	30.05	20.91
7	0.15	48.48	11.21	24.66	24.61	17.10
8	0.15	24.05	3.98	15.21	15.18	10.56
9	0.15	72.07	14.29	23.73	23.67	16.36
10	0.15	24.08	1.79	3.47	3.46	2.41
11	0.15	72.10	1.47	28.61	28.55	19.87
12	0.15	24.07	8.40	25.97	25.91	18.03
13	0.15	24.00	-4.56	37.23	37.13	25.79
14	0.08	264.15	-7.67	40.38	40.03	28.18
15	0.15	72.07	4.34	39.07	39.00	27.08
16	0.15	24.03	2.86	33.75	33.70	23.45
17	0.15	24.07	-3.22	14.40	14.37	9.89
18	0.15	24.05	2.43	21.87	21.83	15.05
19	0.08	240.08	-0.01	29.60	29.53	20.64
20	0.15	24.12	-2.17	5.51	5.51	3.81
21	0.08	120.68	2.18	27.83	27.76	19.40
22	0.08	387.43	-18.81	34.23	34.03	23.20
23	0.15	24.08	0.11	11.63	11.60	7.98
24	0.15	24.03	11.71	30.28	30.24	20.75
25	0.15	24.00	7.46	11.10	11.08	7.64

Table A.2: Cavern Data of the 25 analyzed examples, SI units.